

4-1-2023

The Faroe-Shetland Channel Jet: Structure, Variability, and Driving Mechanisms

L. Chafik
Stockholms universitet

J. Nilsson
Stockholms universitet

T. Rossby
University of Rhode Island

A. Kondetharayil Soman
Stockholms universitet

Follow this and additional works at: <https://digitalcommons.uri.edu/gsofacpubs>

Citation/Publisher Attribution

Chafik, L., J. Nilsson, T. Rossby, and A. Kondetharayil Soman. "The Faroe-Shetland Channel Jet: Structure, Variability, and Driving Mechanisms." *Journal of Geophysical Research: Oceans* 128, 4 (2023). doi: [10.1029/2022JC019083](https://doi.org/10.1029/2022JC019083).

This Article is brought to you by the University of Rhode Island. It has been accepted for inclusion in Graduate School of Oceanography Faculty Publications by an authorized administrator of DigitalCommons@URI. For more information, please contact digitalcommons-group@uri.edu. For permission to reuse copyrighted content, contact the author directly.

The Faroe-Shetland Channel Jet: Structure, Variability, and Driving Mechanisms

Keywords

AMOC; Nordic Seas; overflows

Creative Commons License



This work is licensed under a [Creative Commons Attribution-Noncommercial-No Derivative Works 4.0 License](https://creativecommons.org/licenses/by-nc-nd/4.0/).

The Faroe-Shetland Channel Jet: Structure, Variability, and Driving Mechanisms



Key Points:

- The Faroe-Shetland Channel Jet is a robust feature across ocean reanalyses, both high-resolution and low-resolution
- The deep flows in the Faroe-Shetland Channel are regulated by the wind-forced circulation in the Nordic Seas
- The high-resolution ocean reanalysis, GLORYS12, is a promising product to study the overflow pathways/dynamics in the Nordic Seas





Correspondence to:

L. Chafik,
leon.chafik@misu.su.se

Citation:

Chafik, L., Nilsson, J., Rossby, T., & Kondetharayil Soman, A. (2023). The Faroe-Shetland Channel Jet: Structure, variability, and driving mechanisms. *Journal of Geophysical Research: Oceans*, 128, e2022JC019083. <https://doi.org/10.1029/2022JC019083>

Received 12 JUL 2022
 Accepted 30 MAR 2023

L. Chafik¹ , J. Nilsson¹ , T. Rossby² , and A. Kondetharayil Soman¹ 

¹Department of Meteorology, Stockholm University, Stockholm, Sweden, ²Graduate School of Oceanography, University of Rhode Island, Kingston, RI, USA

Abstract The Faroe-Bank Channel (FBC) is a key gateway through which dense overflow water of the Nordic Seas supplies the lower limb of the Atlantic Meridional Overturning Circulation. Most recently, it was discovered that a deep jet through the Faroe-Shetland Channel carries the bulk of this overflow water, but numerous questions regarding its structure, seasonality, and interannual variability as well as its linkage to atmospheric forcing remain poorly understood. A realistic high-resolution ocean reanalysis (GLORYS12; 1993–2018) is, therefore, employed to address these questions. We first confirm that the Faroe-Shetland Channel Jet is a permanent feature in GLORYS12 as well as in an ensemble of low-resolution reanalyses. On seasonal time scales, we find a strong transport covariability between this deep jet and the observed FBC overflow. On interannual time scales, the strength of this deep jet is governed by the wind-forced circulation in the Nordic Seas. Due to the largely barotropic structure of these flows, they have a signature detectable in satellite sea-surface heights. Further, we suggest that the structure of the deep jet is qualitatively consistent with a geostrophic dynamical model that accounts for along-isobath density variations. This study indicates that GLORYS12 is a promising product to study the dense water pathways and dynamics in the Nordic Seas.

Plain Language Summary Our knowledge about ocean circulation at the sea surface has increased over the past couple of decades thanks to satellite observations. The deep ocean circulation, however, remains poorly understood and requires multiple observational platforms to piece it together. Recently, a rapid current was discovered in a very dynamic region, i.e., the Faroe-Shetland Channel. This deep flow is found to connect to one of the main gateways that feed the deep North Atlantic Ocean with the dense waters of the Nordic Seas, and is, therefore, important for the strength of the Atlantic Meridional Overturning Circulation. We seek here to learn more about its characteristics and drivers using a high-resolution ocean reanalysis, i.e., a model that assimilates ocean observations. When compared to multiple observational platforms, the ocean reanalysis is found to perform reasonably well. The location of this deep jet is confirmed to be robust both in this high-resolution ocean reanalysis as well as in low-resolution ocean reanalyses. We also show that variations in transport of this deep jet are largely governed by the wind field in the Nordic Seas. Because of this, the variations associated with the transport of this deep jet can be detected from satellite-derived sea-surface heights.

1. Introduction

Variations in the volume transport of the Nordic Seas overflow, the flow of cold and dense water at depth, is an important diagnostic of the stability of the Atlantic Meridional Overturning Circulation or AMOC (Chafik & Rossby, 2019; Hansen et al., 2016; Zhang et al., 2011), a climate-regulating ocean circulation transporting heat poleward in the Atlantic Ocean. In essence, the AMOC transports warm surface waters northward (upper limb) and cold deep waters southward (lower limb) (Lozier, 2012). The densest waters of the AMOC lower limb are produced in the Nordic Seas (Chafik & Rossby, 2019; Hansen & Østerhus, 2000; Mauritzen, 1996) via two main processes: (a) water-mass transformation due to gradual heat loss of Atlantic-origin water in the boundary current flowing around the rim of the Nordic Seas and the Arctic Ocean (Eldevik et al., 2009; Mauritzen, 1996), and (b) open-ocean convection in the interior gyres of the western Nordic Seas (Huang et al., 2020). This dense water eventually spills back into the deep North Atlantic across the Greenland-Scotland Ridge (GSR; Figure 1), completing the Nordic Seas overturning process.

The Faroe-Bank Channel (FBC) is the deepest passage across the GSR with a sill depth of ~840 m where this continuous deep flow of about 2 Sv ($1 \text{ Sv} = 10^6 \text{ m}^3 \text{ s}^{-1}$) of cold and dense water flows into the subpolar North

© 2023. The Authors.
 This is an open access article under the terms of the [Creative Commons Attribution-NonCommercial-NoDerivs License](https://creativecommons.org/licenses/by-nc-nd/4.0/), which permits use and distribution in any medium, provided the original work is properly cited, the use is non-commercial and no modifications or adaptations are made.

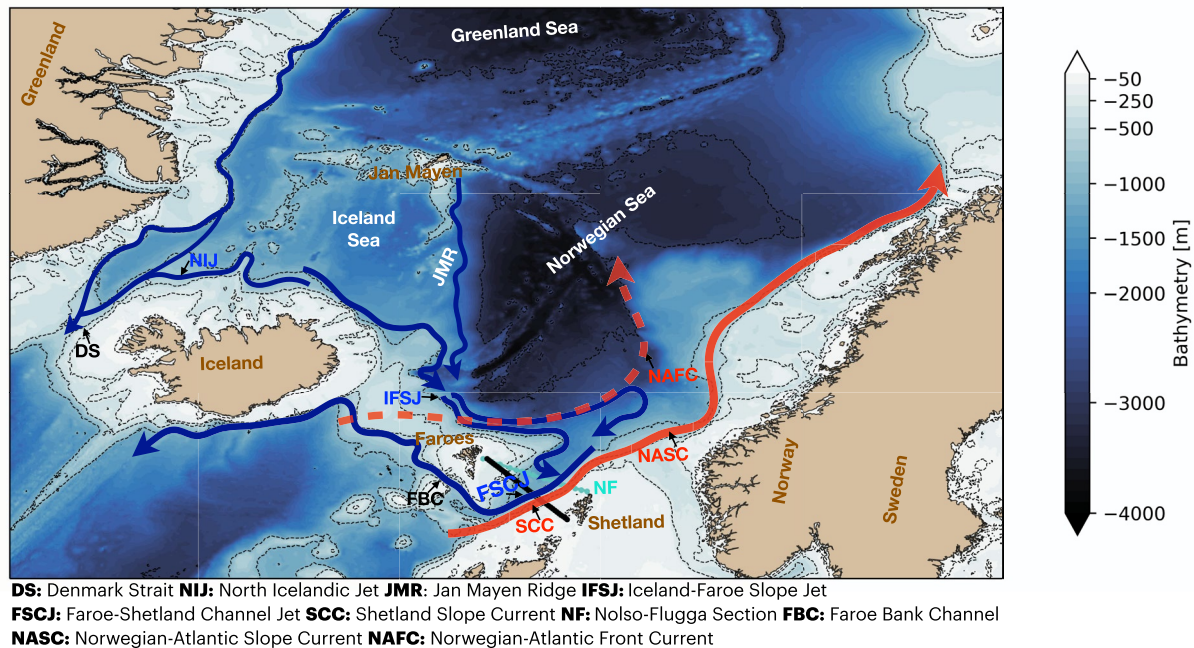


Figure 1. Ocean circulation in the Nordic Seas. The warm surface flow passing the Faroe-Shetland Channel (FSC) and moving polewards is indicated in red. The other warm branch entering the Nordic Seas between the Faroes and Iceland is also indicated (in dashed red for presentation purpose only). The deep pathways transporting overflow water toward the Denmark Strait (DS) between Greenland and Iceland and toward the Faroe-Bank Channel (FBC) are shown in blue. The deep pathway from the Jan Mayen Ridge (JMR) toward the northern slope of the Greenland-Scotland Ridge is also shown. The turquoise section is the Nolso-Flugga (NF) standard hydrographic section. The black section across the FSC represents the transect used for the analyses.

Atlantic (Østerhus et al., 2019). The FBC overflow (FBCO) transport has been monitored continuously since 1995 (Hansen et al., 2016). These measurements have revealed that this deep overflow component of the overturning circulation has remained stable until today, which is consistent with the finding of a stable Atlantic inflow to the Nordic Seas estimated using hydrographic casts that date back to the early 1900s (Rossby et al., 2020). What has been, however, less understood is the upstream (southbound) pathways leading to the FBCO, how they vary over time and through which large-scale forcing mechanisms.

Observational evidence of a deep current tracing the northern slope of the GSR and transporting denser water from the Iceland Sea toward the northern Faroe slope, i.e., the Iceland-Faroe Slope Jet (IFSJ), has recently been reported in Semper et al. (2020). These authors documented the existence of this bottom-intensified current (which has two cores, at 750 and 1,100 m) that had similar hydrographic properties as the FBCO, and showed that it may supply half of the total FBCO, i.e., about 1 Sv. As such, the IFSJ is one of the major pathways of dense water toward the FBCO, which is consistent with the Lagrangian study of Sjøiland et al. (2008). The latter study demonstrated that floats released inshore of the 1,750-m isobath at the northern slope of the GSR, between Iceland and the Faroe Islands, revealed strong topographic control of their movement and approached the Faroe-Shetland Channel (FSC) directly before they exited through the FBC. Chafik et al. (2020) put forward that this direct route to the FBC via the FSC shown by Sjøiland et al. (2008) is not exclusive and that an indirect or longer route toward the Norwegian slope before turning south toward the FSC (see Figure 1), as inferred from observations and confirmed in a high-resolution ocean general circulation model, also contributes to the FBCO. This indirect Norwegian-slope route, which was found to be activated by an anomalously anticyclonic atmospheric circulation over the Nordic Seas, could account for the portion of the FBCO that is not supplied by the IFSJ. Furthermore, Chafik et al. (2020) found that the bulk of the FBCO, which consists of water of both the direct and indirect branch, is transported by a deep rapid flow banked against the eastern slope of the FSC. This deep current, namely the Faroe-Shetland Channel Jet (FSCJ), is now considered the primary conduit of the FBCO in the FSC, but there is much we do not know about its structure, variability, and driving mechanisms. These aspects are the focus of the present study.

An unresolved aspect of the FSCJ is its setting with shallow water to the left in the flow direction (Figure 2). This pathway contradicts previous thinking (Eldevik et al., 2009), and goes against the prediction of cyclonic

A. Time-mean bottom geostrophic flow along f/H contours B. Time-mean bottom geostrophic flow along f/H contours including FSCJ

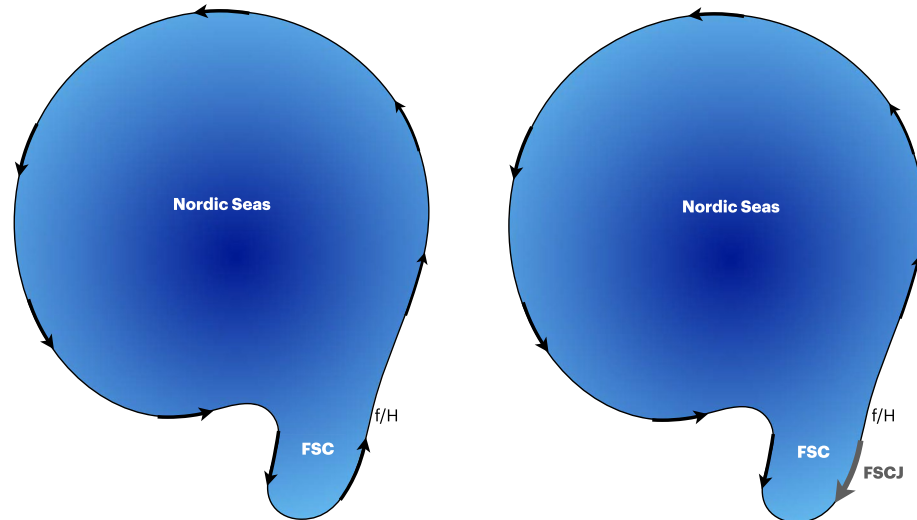


Figure 2. (a) A simplified sketch of the bottom circulation on closed depth contours (or more accurately f/H contours, where f is the Coriolis parameter and H is the depth) as diagnosed from the dynamical model of Nøst and Isachsen (2003). (b) Similar to (a) but including the mean position of the Faroe-Shetland Channel Jet (FSCJ; Chafik et al., 2020). Note that the FSCJ violates the cyclonic bottom circulation expected from cyclonic wind forcing in the Nordic Seas.

near-bottom flow on closed depth contours in the Nordic Seas from the geostrophic model of Nøst and Isachsen (2003). Thus, the location of the FSCJ emerges as a dynamical oddity, similar to the North Icelandic Jet supplying the Denmark Strait overflow (Jonsson & Valdimarsson, 2004; Våge et al., 2011). In the present work, we will use the model of Nøst and Isachsen (2003) to analyze the bottom flow on isobaths that close themselves in the Nordic Seas-Arctic Ocean, i.e., isobaths below the sill in the FBC. We find that the FSCJ can partly be explained by incorporating the effect on the flow of bottom density variations along isobaths (Aaboe & Nøst, 2008; Nilsson et al., 2005). The model we use assumes geostrophic balance and cannot be applied on isobaths near the sill, where nonlinear hydraulic dynamics become important (Yang & Pratt, 2014).

The FSC is a highly dynamical region with pronounced eddy activity (Chafik, 2012; Oey, 1997; Sherwin et al., 1999, 2006). Eddies originating from both north of the Faroes and the Shetland Slope Current (Chafik, 2012) can on short time scales lead to significant undulations of the interface height separating the northward from the southward limb of the AMOC. In the present work, we show that sea-surface height fluctuations in the interior of the FSC are consistent with changes in the deep flows in the region that are dominated by the FSCJ. We also find a striking temporal relationship between the number of coherent anticyclonic eddies (AEs) in the region and FSCJ transport which we do not yet understand and will require further study.

The paper is organized as follows: To set the stage for our analyses, we first validate the ocean reanalysis by comparing it to repeat hydrography in the FSC. We then compare the flow field of the ocean reanalysis to multiple observational platforms before examining the FSCJ variability on multiple time scales and identify associated driving mechanisms. The study ends with a summary and conclusions.

2. Data and Methods

2.1. Ocean Reanalyses

The main ocean reanalysis used in this study is the high-resolution GLORYS12 from the Copernicus Marine Environment Monitoring Service (CMEMS). The GLORYS12 ocean reanalysis (Jean-Michel et al., 2021) is a global eddy-resolving reanalysis with a horizontal resolution of $1/12^\circ$ (about 9.25 km at the equator and 4.5 km at subpolar latitudes) and 50 vertical levels (from 0.5 to 5,700 m with four levels between 600 and 1,100 m). The model component is the NEMO version 3.1 and is driven at the surface by ERA-Interim reanalysis from ECMWF. ETOPO1 bottom topography is used for deep oceans and GEBCO8 on the coasts and continental shelves. We utilize the monthly potential temperature, salinity, zonal velocity, meridional velocity, and sea-surface heights,

covering the 1993–2018 period (the reanalysis starts in 1993 as sea-surface height data from altimetry is a key variable that is assimilated). We compare the mean velocity field in the FSC from GLORYS12 to an ensemble of ocean reanalyses that include four members each with a different ocean model and span the 1993–2017 period. These models (GLORYS2V4, ORAS5, GloSea5, and V-GLORS05) have a horizontal resolution of $1/4^\circ$ (~ 24 km) and 75 vertical levels (from 0.5 to nearly 6,000-m depth).

2.2. Transport Calculation

We use the GLORYS12 velocities across the FSC to calculate the deep southward transport as follows:

$$\Psi = \int_{-h(x)}^{600} \int_0^L v(x, z) dz dx \quad (1)$$

where v is the along-channel velocity component, L is the width of section, x and z are the section distance and depth, respectively, and $h(x)$ refers to bottom depth. This flux calculation is done for the full section, i.e., from the eastern Shetland slope to the western Faroe slope (hereafter deep FSC), as well as for the eastern part of the channel where the FSCJ dominates (hereafter just FSCJ). The western limit of the FSCJ is determined based on the leading Empirical Orthogonal Function mode of the velocities in the FSC, which shows a sign change close to this limit (located near the deepest part of the FSC, not shown). For the upper limit, we use the 600-m depth since it nearly coincides with the time-mean 28.0 kg m^{-3} isopycnal or 0°C isotherm (cf. Figure 3). Through this definition, we are able to calculate the transport associated with the Arctic-origin overflow water found in the deepest part of the FBC (Hansen & Østerhus, 2000; Huang et al., 2020). It should, however, be mentioned that using a variable interface of the 27.8 kg m^{-3} isopycnal does not change the temporal variability of the FSCJ transport calculated following Equation 1 but it increases the mean transport from 1.84 ± 0.70 to 2.00 ± 0.75 Sv (see also Section 3.3).

2.3. Nolso-Flugga (NF) Standard Hydrographic Section

The time-mean hydrographic data including in situ temperature and salinity from the NF standard hydrographic section in the FSC (Larsen et al., 2018), Figure 1, are used to validate the water-mass structure (temperature, salinity, and density) of GLORYS12. The data consist of CTD (conductivity-temperature-depth) and/or STD (salinity-temperature-depth) profiles that have been collected since 1988–2021 by Marine Scotland and the Faroe Marine Research Institute. The data are in 1-m depth bins and have been quality controlled by the originator before its use in this study. Out of the 187 hydrographic sections (1988–2021), the western FSC has been occupied nearly twice as much as the eastern side. As such the data are not as smooth on the Shetland slope, which one limitation of the observed hydrography.

2.4. Observed FBCO Transport

We use the kinematic overflow transport through the FBC that is derived solely from the velocity field and has been made available by the Faroe Marine Research Institute. More details about this transport time series can be found in Hansen et al. (2016) but a short summary is provided here. Since November 1995, the overflow through the narrow FBC has been monitored continuously through an Acoustic Doppler Current Profiler (ADCP) mooring deployed in the middle of the channel. Apart from an annual maintenance service of 3 weeks during May or June, the overflow time series is complete. The missing weeks are being accounted for in the present study by excluding months with data fewer than 20 days. The 1996–2018 daily FBCO time series used herein has been monthly averaged before the analysis. It should also be mentioned that according to Østerhus et al. (2019), the average kinematic FBCO estimate between 1995 and 2015 of 2.1 Sv includes 0.2 Sv of waters less dense than the commonly used criterion of $\sigma_0 > 27.8 \text{ kg m}^{-3}$.

2.5. Argo Floats

We searched for Argo floats deployed in the Nordic Seas that exited through the FBC using argopy software (Maze & Balem, 2020), and found three that met this criterion. All floats have identification numbers (WMO ID) allocated depending upon platform type and deployment area (see Table 1). The tracks of the Argo floats are

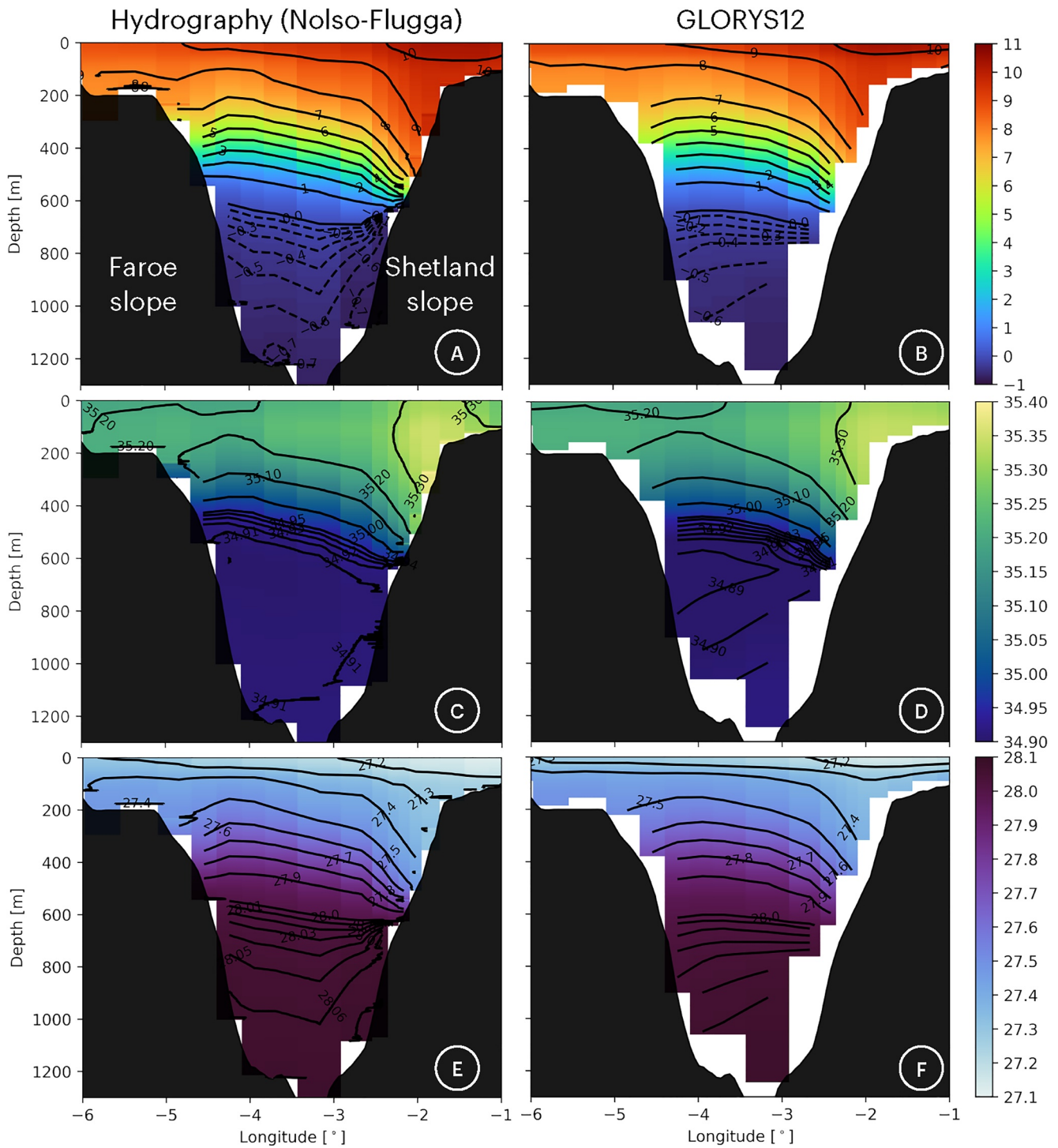


Figure 3. The climatological temperature ($^{\circ}\text{C}$) in the FSC at the Nolso-Flugga section from (a) repeat hydrography (1988–2021) and (b) GLORYS12 ocean reanalysis (1993–2018). (c and d) Same as (a) and (b) but for salinity. (e and f) Same as (a) and (b) but for density (kg m^{-3}).

compared to the time-mean bottom velocity field from the ocean reanalysis. Note that the tracks of the Argo floats are independent of the velocity field of GLORYS12.

Table 1
The Argo Floats Used in This Study; Their WMO Numbers, Abbreviations, and Their Active Periods

WMO number	Abbreviation	Start date, position	End date, position
6900344	AF69	2005-10-16, Iceland Sea	2011-04-18, Labrador Sea
3901864	AF39	2016-09-09, Norwegian Basin	2020-10-08, eastern Subpolar North Atlantic
7900176	AF79	2007-08-31, Iceland Sea	2011-12-08, southern slope of GSR

2.6. Satellite Altimetry and ERA-Interim

We use absolute dynamic topography or sea-surface heights derived from satellite altimetry (1993–2020) by Taburet et al. (2019) and retrieved from the Copernicus Marine Service (CMEMS). The daily sea-surface height data are averaged into monthly fields, detrended, and deseasoned to calculate the anomalies. For the mean sea-level pressure, we use the ERA-Interim data (1993–2018), which has also been detrended and deseasoned prior to the analysis. More information about this data set can be found in Dee et al. (2011). The daily mean sea-level pressure anomaly fields have also been used to derive the storm tracks by calculating the standard deviation of the 2–6 days bandpass-filtered maps (Woollings et al., 2012).

2.7. Eddy Detection

To detect coherent eddies, we utilize the multimission altimetry-derived eddy trajectories version 3.2 DT (AVISO) computed with the “all satellites” constellation maps distributed by AVISO+ (Pegliasco et al., 2022). This atlas uses absolute dynamic topography data with a spatial resolution of $1/4^\circ$ for eddy detection and tracking. This data set provides the tracks of anticyclonic and cyclonic eddies, with their location, contours, amplitudes, radius, speeds, and metadata from 1993 to present. The underlying eddy detection algorithm behind this product is py-eddy-tracker (PET) developed by Mason et al. (2014), and it has been further optimized by Pegliasco et al. (2022) for handling large data sets. According to Chelton et al. (1998), the baroclinic Rossby radius of deformation is around 10 km in the FSC region. Therefore, the altimetry data does not resolve all the mesoscale eddies in our domain. Though we miss out on the smaller eddies, we are able to get a sense of the year-to-year variability of eddy generation/formation, and hence eddy count per year.

3. Results and Discussion

3.1. Temperature and Salinity Distributions

Figure 3 examines how well GLORYS12 captures the FSC climatological temperature, salinity, and density structure as compared to repeat hydrography (1988–2021) from the NF section (Larsen et al., 2018). The highest temperatures and salinities are found in the upper-ocean on the Shetland slope (see Figure 1). These waters correspond to North Atlantic Water (NAW; $T > 9.5^\circ\text{C}$, $S > 35.3$) that characterize the Shetland Slope Current (Berx et al., 2013; Chafik, 2012; McKenna et al., 2016). On the Faroe slope, the temperatures and salinities are slightly lower and the water masses correspond to Modified North Atlantic Water (MNAW; $7 < T < 8.5^\circ\text{C}$, $35.1 < S < 35.3$). More details about these water masses can be found in Hansen and Østerhus (2000) and McKenna et al. (2016). At depths below 600 m, the temperatures drop below 0°C and the waters become fresher and denser—here flow the deep dense waters of the Nordic Seas (Norwegian Sea Arctic Intermediate Water, $-0.5 < T < 0.5^\circ\text{C}$, $34.87 < S < 34.9$, and Norwegian Sea Deep Water, $T < -0.5^\circ\text{C}$, $S = 34.91$) that eventually feed the FBCO. The density structure at greater depths, in both the hydrography and the ocean reanalysis, is sloping down toward the Faroe slope. The strongly sloping isopycnals at depth on the Shetland side from hydrography (note that the isopycnals are less steep in GLORYS12 at this section) are consistent with the existence of a strong southward-flowing current, i.e., the FSCJ. This structure at depth on the Shetland slope is shown for the first time from repeat hydrography.

Figure 4 shows the density biases calculated as repeat hydrography from the NF section (1988–2021) minus GLORYS12 (1993–2018). In the upper-ocean, the water masses are warmer in observed hydrography and hence generally less dense as compared to GLORYS12. At intermediate depths, the water masses from observed hydrography are denser as compared to GLORYS12. This bias is noticeably smaller at greater depths, although on the Shetland side, GLORYS12 is slightly denser as compared to observed hydrography. This evaluation (Figures 3

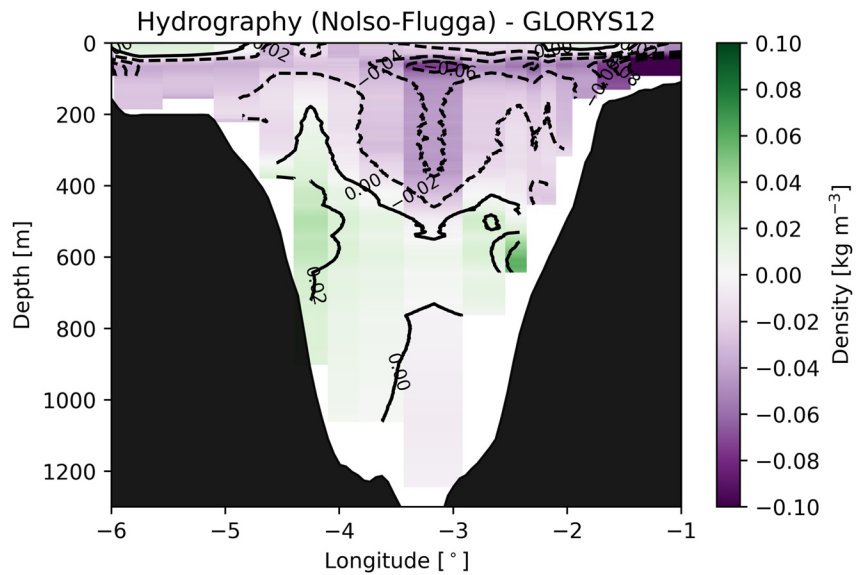


Figure 4. Potential density bias (kg m^{-3}) calculated as hydrography from the Nolso-Flugga hydrographic section (1988–2021) minus GLORYS12 (1993–2018).

and 4) indicates that the GLORYS12 water-mass structure and properties are generally consistent with those identified from repeat hydrographic surveys across the FSC (McKenna et al., 2016).

3.2. Time-Mean Flow Structure

While water-mass properties throughout the water column can be evaluated using repeat hydrography, no product exists for the time-mean deep circulation in the FSC. Figure 5 shows the time-mean velocities below 600 m in the eastern Nordic Seas overlaid by three Argo float trajectories, that exited the Nordic Seas into the North Atlantic through the FBC. The large-scale deep circulation in the Nordic Seas is mainly cyclonic, which is in

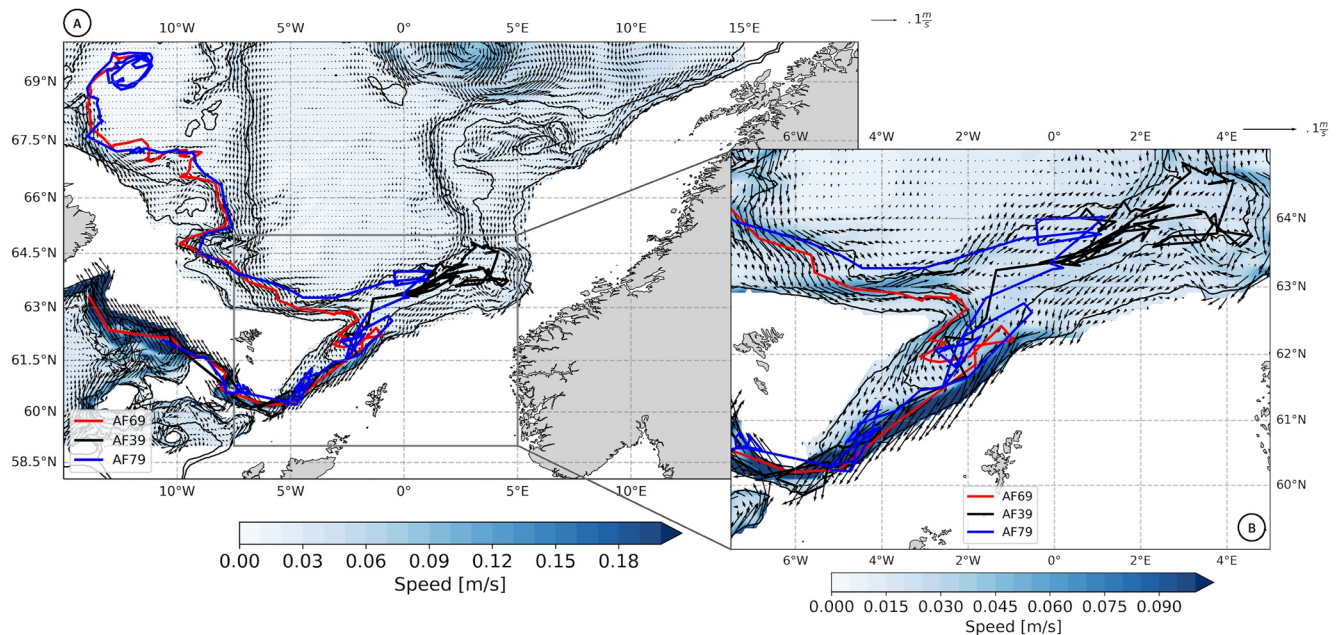


Figure 5. The time-mean deep velocity (arrows) and speed (colors) fields as averaged below 600 m for 1993–2018 from the GLORYS12 ocean reanalysis. The fields are overlaid by the pathways of three ARGO floats traveling southwards through the Faroe-Shetland Channel (FSC) at different times during the period (see Table 1). The black contours depict the 800-m, 1,400-m, and 2,400-m isobaths. (b) Same as (a) but the map zooms into the FSC region and the speed has been adjusted.

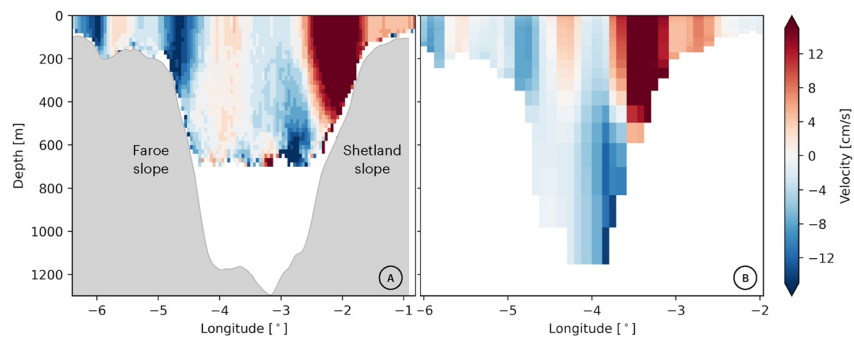


Figure 6. Along-channel time-mean velocity field from (a) ship-mounted Acoustic Doppler Current Profiler (ADCP; 2008–2016) and (b) GLORYS12 ocean reanalysis (1993–2018). Positive/negative values denote northward/southward velocities. Note that the GLORYS12 transect (see Figure 1) is slightly different from that based on ship-mounted ADCP. More details can be found in Chafik et al. (2020), Rossby and Flagg (2012), and Rossby et al. (2018).

agreement with the contribution from the strong cyclonic wind forcing in the Nordic Seas as diagnosed from simple geostrophic dynamics (Nøst & Isachsen, 2003; Timmermans & Marshall, 2020). Many of the known features of the deep circulation seem to be present in the GLORYS12 product: the southward flow along the Jan Mayen Ridge (JMR), the eastward flow of the IFSJ from north of Iceland toward the FSC along the northern slope of the GSR, and the southward-flowing FSCJ along the Shetland slope. The flow along the JMR traces deeper isobaths or f/H contours and joins the IFSJ east of Iceland, from where they flow together toward the FSC. Right north of the Faroes this joint flow splits again: one path turning directly into the FSC and one traces the deeper isobaths toward the Norwegian Sea (along the Norwegian Atlantic Front Current, see Figure 1). In the FSC, bottom currents are present along both sides of the channel but are weak in a time-mean sense on the Faroe side, while the FSCJ that is banked against the Shetland slope is consistently strong. The IFSJ evidently crosses over to the FSC and coalesces with the FSCJ. As such, the FSCJ is the main flow branch that eventually feeds the FBCO.

The paths of the Argo floats (cf. Figure 5) closely trace the time-mean deep circulation as deduced GLORYS12 (1993–2018). The Argo floats spend most of their time at a depth of about 1 km. Two floats (AF69 and AF79) track each other closely from the interior of the Iceland Sea and later along the northern slope of the GSR. North of the Faroes, however, FSC paths diverge following the mean flow: the first of the two (red track), which traced shallower isobaths, entered directly into the channel from the north of the Faroes, while the other float (blue track) located at deeper isobaths north of the Faroes, followed a path toward the Norwegian slope. The behavior of the floats north of the Faroes is similar to that of the RAFOS floats shown by Sjøiland et al. (2008) as well as the model-based Lagrangian particles in Chafik et al. (2020). The third float (AF39; black track) spends time off the Norwegian slope before eventually also finding its way into the FSC. Note that all three floats eventually flow on the eastern side of the FSC following the FSCJ toward the FBC. A similar behavior was observed from the cluster of floats released north of the Iceland-Faroe-Ridge that later escaped through the FBC via the FSC (Sjøiland et al., 2008). Overall, the pathways of the three Argo floats are not inconsistent with the GLORYS12 time-mean velocity field, especially with regard to the newly discovered deep jets (Chafik et al., 2020; Semper et al., 2020).

Next, we confirm that the ocean reanalysis accurately reproduces the velocity field across the FSC. Figure 6 shows the time-mean along-channel velocity field from ship-mounted ADCP (2008–2016) and GLORYS12 (1993–2018). To a large extent, the time-mean velocity field from the high-resolution ocean reanalysis is strikingly similar to the ADCP observations in both structure and strength although the ship-mounted ADCP does not extend deeper than ~600 m. Both observations and reanalysis capture a southward upper-ocean flow on the Faroe slope, the poleward Shetland Slope Current in the upper layers, and most importantly the deep core of the FSCJ on the Shetland side. Furthermore, the ocean reanalysis shows the FSCJ core banked against the Shetland slope at depth and extending up to middepths (~500 m). This bottom intensification is evident in the ADCP measurements. The high velocities associated with the FSCJ have also been observed using an ADCP mooring close to the Shetland slope (cf. Chafik et al., 2020), their Figure 6b. It should, however, be noted that the mid-depth core of the FSCJ that was apparent in the ocean model used by Chafik et al. (2020), their Figure 5, is less clear in GLORYS12.

We now assess whether ocean reanalyses of coarser-resolution capture the main flow structure in the FSC (see Section 2.1 for more details about these coarse-resolution ocean reanalyses). This analysis is important to

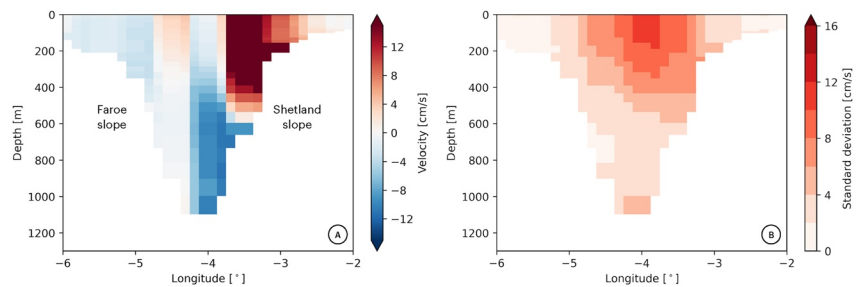


Figure 7. (a) The time-mean ensemble mean of the velocity field in the Faroe-Shetland Channel for the 1993–2017 period from coarse-resolution ocean reanalyses (GLORYS2V4, ORAS5, GloSea5, and V-GLORS05; see Section 2.1) and (b) the standard deviation of the ensemble members.

establish that the position of the FSCJ in the ocean reanalyses does not depend on resolution. Figure 7 shows the ensemble time-mean and standard deviation of this set of ocean reanalyses, see Section 2, and demonstrates that the velocity structure (Figure 7a) is largely similar to that from the high-resolution GLORYS12 ocean reanalysis, but in the coarser-resolution ocean reanalyses the velocities are weaker. Moreover, the southward flow on the Faroe side is weak; a consistent feature across these coarse-resolution ocean reanalyses. Their ensemble standard deviation (Figure 7b) further indicates that the largest variation between the different ocean reanalyses occurs in the upper and central parts of the channel (similar to the bias structure seen in Figure 4), but less so in the vicinity of the FSCJ. This indicates that the low-resolution ocean reanalyses agree to a large extent on the position of the FSCJ. These results thus show that the position of the FSCJ under the main Atlantic inflow core is a robust feature across ocean reanalyses, and further in agreement with the along-channel geostrophic velocities calculated from hydrography and altimetry across the FSC (Berk et al., 2013).

3.3. The Deep Flows on Seasonal Time Scales

Figure 8 shows the seasonally averaged velocities (DJF, MAM, JJA, and SON) from GLORYS12 below 600 m in our region of interest. The spatial seasonal patterns indicate that the velocities along the FSCJ toward the FBCO are enhanced during summer as compared to winter (cf. Figure 9). This is, however, in contrast to the deep flow north of the Faroes or the IFSJ (tracing the 1,400-m isobath) as well as the deep flow along the JMR (tracing the 2,400-m isobath). The strength of the IFSJ as well as the JMR deep flow exhibits a seasonality that is likely a response to the large-scale wind field in the Nordic Seas (see, e.g., Bringedal et al., 2018). During the summer months (JJA), the winds are weak and the IFSJ and flow along the Mayen Ridge are weak, while during the winter months (DJF), the IFSJ strengthens and reaches its maximum (cf. upper panels in Figure 8). This seasonality from GLORYS12 is similar to that based on the ADCP mooring north of the Faroes (Chafik et al., 2020; Semper et al., 2020).

We now quantify and compare the seasonal cycle of the volume transport related to the deep flows. Figure 9 shows the seasonal cycle of the observed FBCO (green), the FSCJ transport from GLORYS12 (blue), and the deep FSC transport from GLORYS12 (dashed purple line). Both the observed and modeled transport exhibit a clear seasonal cycle, with minimum in March and maximum from June to October. An important aspect of the seasonal cycle shown in Figure 9 is that the deep FSC transport matches the annual cycle of the FBCO transport cycle better than the FSCJ alone. This suggests that even if the FSCJ dominates the total deep transport in the FSC, the transport on the western Faroe side is not entirely negligible. The mean and standard deviation of the western transport are 0.45 ± 0.41 Sv, compared to 1.84 ± 0.70 Sv of the FSCJ. Together, they sum up to 2.29 ± 0.83 Sv, which is close to the 2.17 ± 0.35 Sv observed FBCO estimate (Hansen et al., 2016). Note, however, that the mean transport based on a variable interface of the $\sigma_0 > 27.8 \text{ kg m}^{-3}$ isopycnal is 2.61 ± 0.38 Sv, indicating that GLORYS overestimates the time-mean deep flows in the FSC based on this criterion.

The deep FSC transport from GLORYS12 is found to agree well, with regard to the amplitude of the seasonal cycle, with the observed seasonality of the FBCO transport. However, the correlation between the respective seasonal cycles is somewhat less than that based on the FSCJ transport (0.85 versus 0.88). The phasing of the seasonal cycle of the FSCJ transport is thus better aligned with the FBCO. As demonstrated in Figure 9, both the observed FBCO and the FSCJ transport from GLORYS are anomalously northward in winter (weak transport) and anomalously southward in

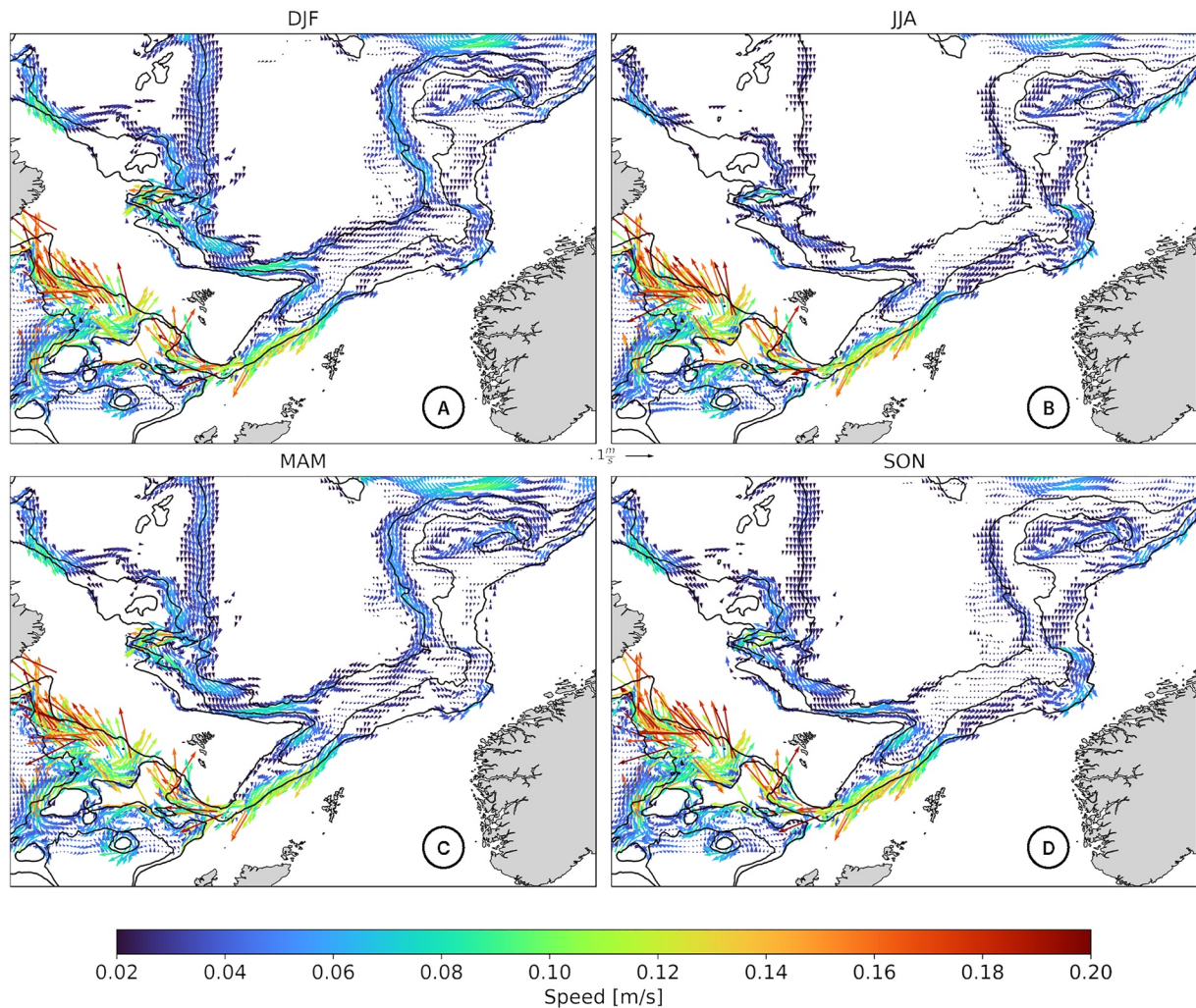


Figure 8. The seasonally averaged flow below 600 m. The vectors indicate the strength and direction of the flow. The colors indicate the magnitude of the flow. Speeds <0.02 m/s have been masked. The black contours depict the 800-m, 1,400-m, and 2,400-m isobaths.

summer (strong transport). This structure is less clear for the deep FSC, especially between October and December. The main point is that this analysis confirms the strong seasonal covariability between the FSCJ and the FBCO.

3.4. The Deep Flows on Interannual Time Scales

Figure 10 shows interannual transport anomalies of the FSCJ (blue) and the deep FSC (purple) from the GLORYS12 ocean reanalysis as well as the observed FBCO (green; 1996–2018). The correlation coefficient between the FSCJ transport and the observed FBCO transport (1996–2018) on these time scales is 0.41. However, by including the transport on the Faroe side, the correlation between the deep FSC transport and the FBCO is improved (0.51). This is expected since the FBCO is fed by the entire deep FSC transport. Note, however, that it is the FSCJ component that explains the majority of the variance of the observed FBCO transport. On interannual time scales, the standard deviation of the FBCO is ± 0.13 Sv, which is more similar to that of the deep FSC transport anomaly, i.e., ± 0.16 Sv, while that associated with the FSCJ is higher (± 0.24 Sv).

Another aspect worth highlighting regarding the time series shown in Figure 10 is the time lag between the FSCJ (deep FSC) transport and the observed FBCO transport before and after 2005. While the transport time series are more synchronized before 2005, the FSCJ transport (deep FSC) appears to be leading in time between 2005 and 2014 before a possible return to a more synchronized behavior after 2014 is seen. In fact, the correlation coefficient between the FSCJ (deep FSC) and the FBCO during the 1996–2005 period is 0.52 (0.70), while during the 2006–2018 period, the correlation is significantly lower, i.e., 0.34 (0.38). A possible explanation for this nonstationary relationship could

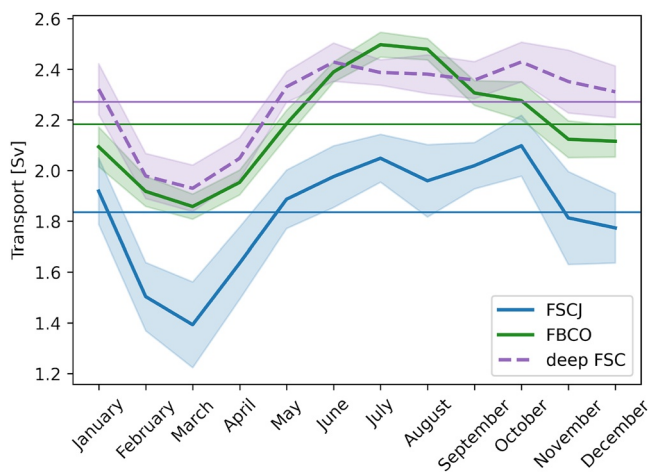


Figure 9. The climatological seasonal cycle of the observed FBC overflow (FBCO) transport (green), the GLORYS12 FSCJ transport (blue), and the GLORYS12 total transport of the Faroe-Shetland Channel (FSC) below 600 m (dashed purple line), i.e., the sum of the Faroe-Shetland Channel Jet and the western deep FSC transports. The shading denotes the standard error of the mean. The horizontal lines show the time-mean of the respective transports. Recall that the calculations of the FBCO and the GLORYS transports use different criteria (see Section 2.2).

be a shift from a period of strong to weak wind forcing and hence a change from barotropic to baroclinic forcing mechanisms after 2005. This is in line with the results and explanation of the weak relationship between sea-surface heights and FBCO variability on interannual time scales reported by Bringedal et al. (2018).

Figure 11 shows how well, on interannual time scales, the transports of the FSCJ (Figure 11a) and the deep FSC (Figure 11b) correlate with the entire velocity field across the FSC. The spatial correlation pattern reveals a fairly barotropic structure and demonstrates a strong anticorrelation in the top-to-bottom velocity field between the eastern and the western parts of the FSC. This barotropic velocity structure must therefore have a signature detectable in sea-surface height gradient across the FSC. In fact, the FSCJ transport variability is not only correlated with the local sea-surface height but is connected to a large-scale sea-surface height signature in the eastern Nordic Seas: Figure 11c shows the pattern resulting when sea-surface heights are regressed onto the FSCJ transport (the regression analysis based on the deep FSC transport yields a similar pattern). This large-scale correlation pattern, which tends to be aligned with the bathymetry, suggests that periods with strong (weak) FSCJ transport coincide with generally higher (lower) sea level in the eastern Nordic Seas: via geostrophy this implies that the prevailing boundary currents along the Norwegian continental margin are weaker (stronger) than normal. This is in agreement with the observational findings of Chafik et al. (2020) and Hátún et al. (2021), where enhanced FBCO transport was reported to coincide with anomalously weak barotropic circulation along the depth contours in the Norwegian Sea gyre. These results

thus suggest that the water-mass pathways in the deep FSC are strongly interconnected and regulated by the wind-forced circulation in the Nordic Seas.

To further demonstrate the close correspondence between sea-surface heights in the FSC interior and the transport of the deep flows, we show their temporal variability in Figure 12. The sea-surface height in the FSC interior (see the location of the blue cross in Figure 10) can be seen to strongly covary with the deep flows feeding the FBCO, such that an enhanced transport at depth in the FSC is consistent with a sea-level increase and a development of a local anticyclonic circulation anomaly. Although at this point this finding is not surprising because of the fairly barotropic structure revealed earlier, it connects for the first time the curious development of pronounced sea level or circulation anomalies in the channel interior to changes in the deep flows. As such, sea-surface height variations in the FSC interior are inherently linked to top-to-bottom flow changes including the FBCO system. Note also that this local relationship between sea-surface heights and deep flows in the FSC is different in terms of locality from that based on the spatial correlation pattern shown in Hátún et al. (2021), their Figure 8, between altimetry and FBCO transport.

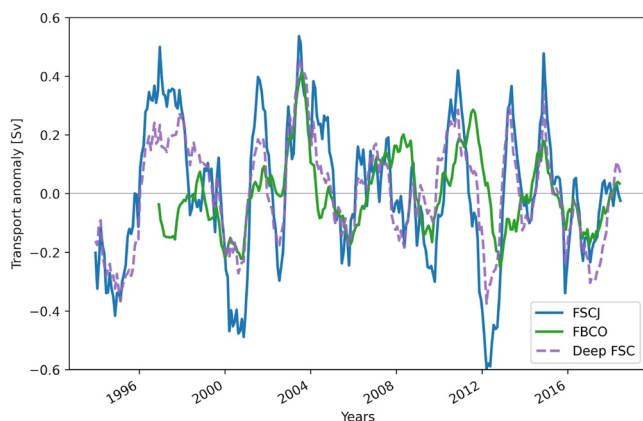


Figure 10. Interannual transport variability of the Faroe-Shetland Channel Jet (blue), deep Faroe-Shetland Channel (dashed purple), and the observed FBCO (green). The time series have been deseasoned and detrended before applying a 12-month running mean to reflect interannual time scales.

3.5. Large-Scale Atmospheric Patterns Associated With the FSCJ

Since the vertically integrated flow on closed depth contours in the Nordic Seas is principally wind driven (Nøst & Isachsen, 2003), we expect the deep flows to respond to variations in the large-scale atmospheric circulation and cyclone activity or storm tracks in the North Atlantic on interannual time scales. By regressing the mean sea-level pressure anomaly onto the transport variability of the FSCJ (Figure 13a), we show that the large-scale atmospheric circulation pattern projects onto the negative North Atlantic Oscillation as signified by a high-pressure and a low-pressure anomaly at higher and lower latitudes, respectively (the regression pattern for the deep FSC shows virtually the same pattern, not shown). Figure 13b demonstrates that the region of low and high baroclinicity (or cyclone activity) of the atmospheric circulation is located within the Nordic Seas and southwest of Europe,

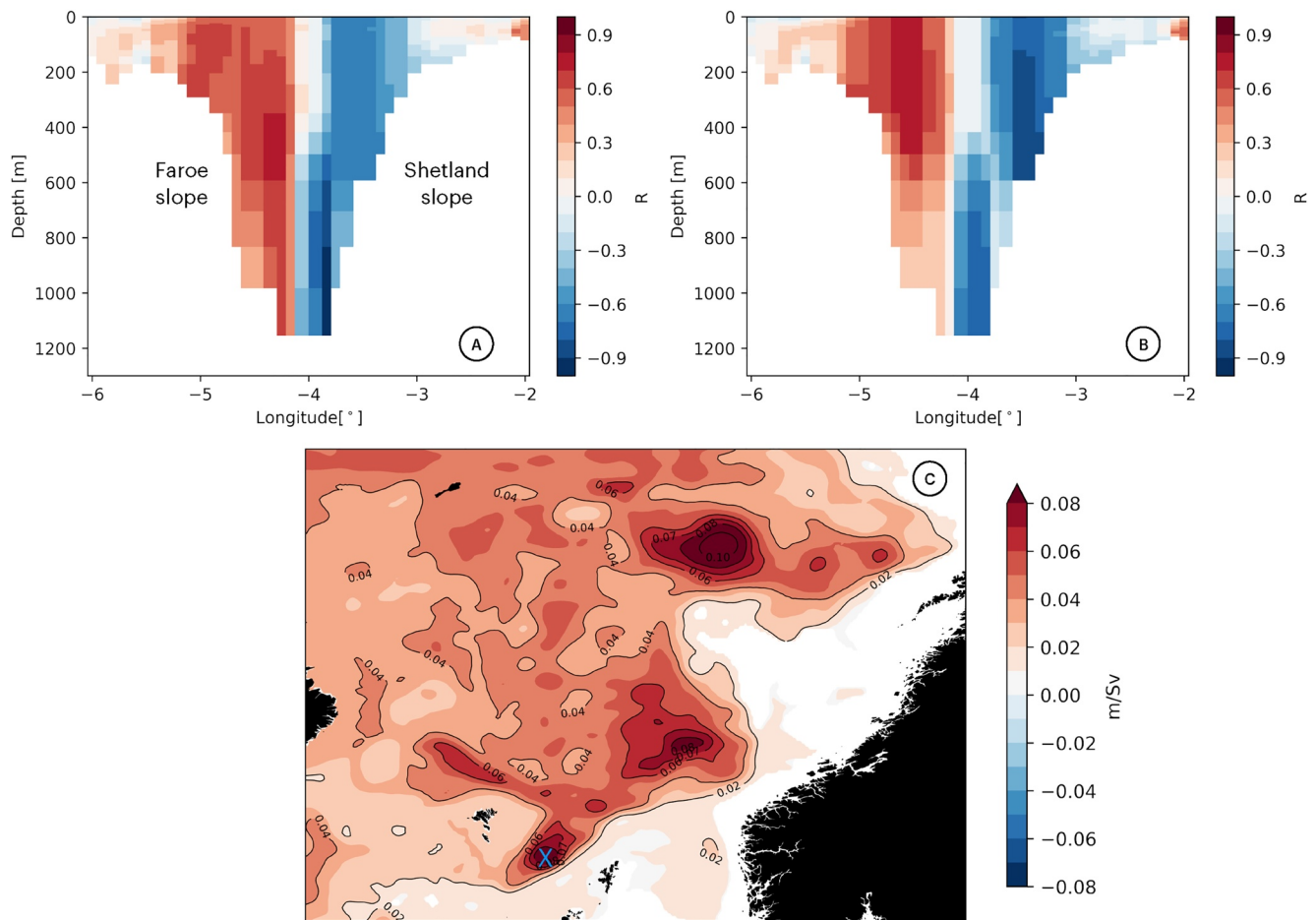


Figure 11. Correlation fields based on velocities in the Faroe-Shetland Channel (FSC) and transport anomalies of (a) the Faroe-Shetland Channel Jet (FSCJ) and (b) deep FSC. (c) Spatial regression patterns (m per Sv) of the sea-surface heights onto the FSCJ transport variations. The white regions indicate nonsignificance at the 95% confidence level assessed using a two-sided t -test. The data have been deseasoned, detrended, and a 12-month running mean was applied before the correlation/regression analysis. The blue cross shows the location of the time series used in Figure 12.

respectively, as would be expected from a negative North Atlantic Oscillation and a southward shift in the main storm tracks (typically oriented northeastwards into the Nordic Seas).

Note, however, that the center of action of the high-pressure anomaly (within the Nordic Seas) is shifted farther north in the Nordic Seas as compared to the climatological position of the Icelandic Low (cf. Figure 13). Similarly, the low-pressure anomaly is shifted to the north of the Azores High climatological position. These results suggest that an increase in the FSCJ transport is associated with anomalously anticyclonic wind conditions in the interior Nordic Seas and Arctic Ocean, corresponding to a decrease in baroclinicity (Figure 13b) as a result of a southward shift in the storm tracks. Such conditions relax the Norwegian Sea gyre circulation, leading to weaker poleward (Atlantic Water) boundary currents, and anomalously strong southward deep flow along the Norwegian slope, which, in turn, enhances the southward transport of the FSCJ (cf. the barotropic structure, Figure 11), and as expected also the FBCO. This response of the bottom circulation to anomalously strong and weak Nordic Seas circulation is summarized in Figure 14. This conclusion is consistent with the results of Yang and Pratt (2013). They studied the Nordic Seas overflow dynamics using an idealized numerical model and found that anticyclonic (cyclonic) large-scale wind forcing indeed enhances (reduces) the overflow.

3.6. Is There a Role for Coherent AEs?

Eddies are able to exchange water across fH contours and hence may transport deep water toward the FSCJ. It is thus of interest to shed some light on the relationship between the generation of eddies and the FSCJ transport. By examining coherent eddies generated in the FSC region from the AVISO Atlas (Pegliasco et al., 2022), a

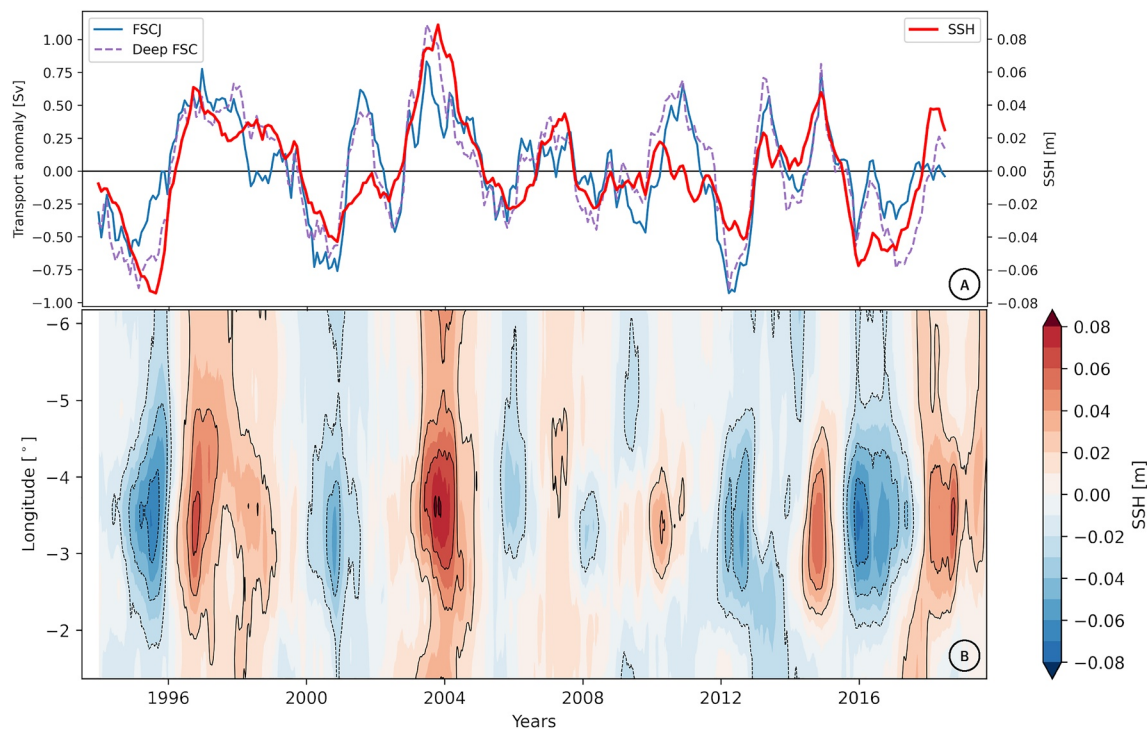


Figure 12. (a) Transport variability of the Faroe-Shetland Channel Jet (FSCJ; blue), deep Faroe-Shetland Channel (FSC; dashed purple) and sea-surface height in the FSC interior (red). The correlation coefficient between the FSCJ/deep FSC transport and the sea-surface is 0.69/0.82. (b) Hovmöller diagram of the sea-surface height anomaly across the FSC. Superimposed are contours for every 0.02 m. In both panels, the data have been deseasoned and detrended before applying a 12-month running mean.

total of 127 AEs that persisted for at least a week in the FSC were detected and counted during the 1993–2018 period, Figure 15. The correlation between the yearly count of AEs with the FSCJ transport is 0.73 (Figure 15a). However, it is interesting to note that the number of AEs covaried simultaneously with the FSCJ transport until 2004 (the correlation during this period is 0.88) and hence also with the top-to-bottom Nordic Seas circulation (Chafik et al., 2020; Hátún et al., 2021), before a lag of 1 year (AEs leading the FSCJ) was observed thereafter. This analysis was repeated for cyclonic eddies but their relationship to the FSCJ transport variability was found to be weak (-0.06 ; not shown) and therefore not discussed further.

During years with strong FSCJ transport (Figure 15b), AEs are observed to populate the Norwegian Basin and dominate the FSC more so than during years with weak FSCJ transport (Figure 15c). This is evident from the difference between strong and weak states of the FSCJ transport (Figure 15d). While the presence of AEs in

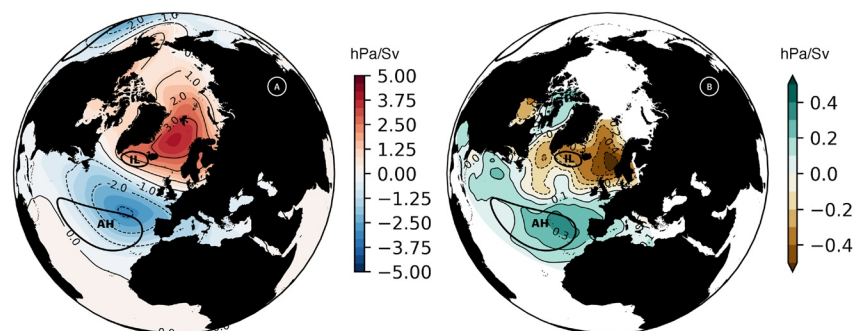


Figure 13. Spatial regression patterns (hPa per Sv) of (a) mean sea-level pressure anomaly and (b) storm tracks onto transport variations of the Faroe-Shetland Channel Jet. The thick contours represent the climatological position of the Icelandic Low (IL) and the Azores High (AH). The storm track or cyclone activity is calculated as the standard deviation of 2–6-day bandpass-filtered daily sea-level pressure. The data have been deseasoned, detrended and a 12-month running mean was applied before the regression analysis.

A. Anomalous bottom geostrophic flow during strong wind forcing B. Anomalous bottom geostrophic flow during weak wind forcing

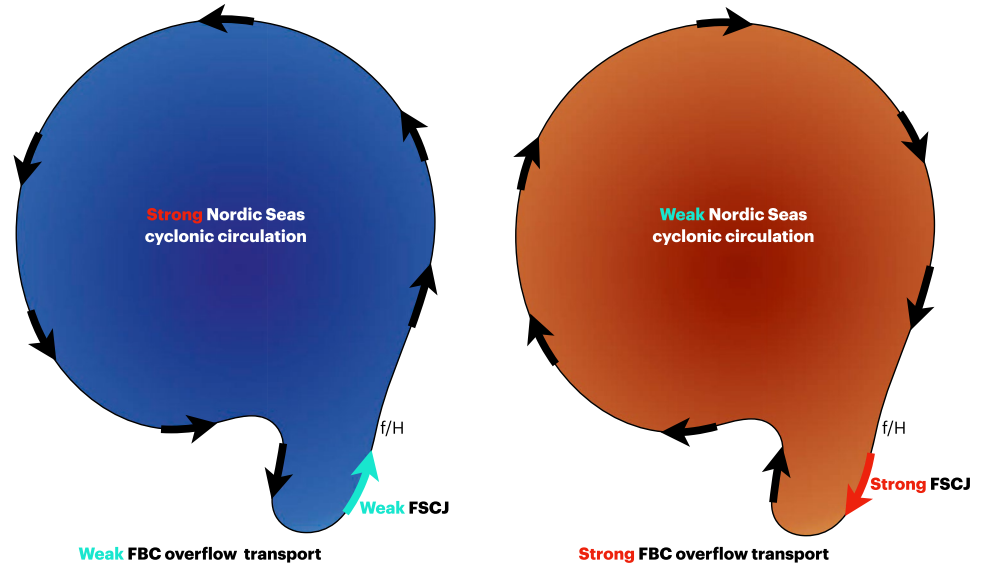


Figure 14. A sketch of the bottom circulation anomaly during anomalously (a) cyclonic/strong and (b) anticyclonic/weak Nordic Seas circulation. Note that the Faroe-Shetland Channel Jet transport and hence that of the FBC overflow are enhanced during anomalously weak cyclonic circulation.

the FSC generally result in a deepening and increased tilt of the isopycnals, which via geostrophy, strengthens the FSCJ transport, we cannot at this stage make any mechanistic inferences about cause and effect. In conclusion, we show that enhanced presence of AEs is consistent with strengthened FSCJ transport, but whether they also lead to greater overflow, and by what dynamics, will need further study.

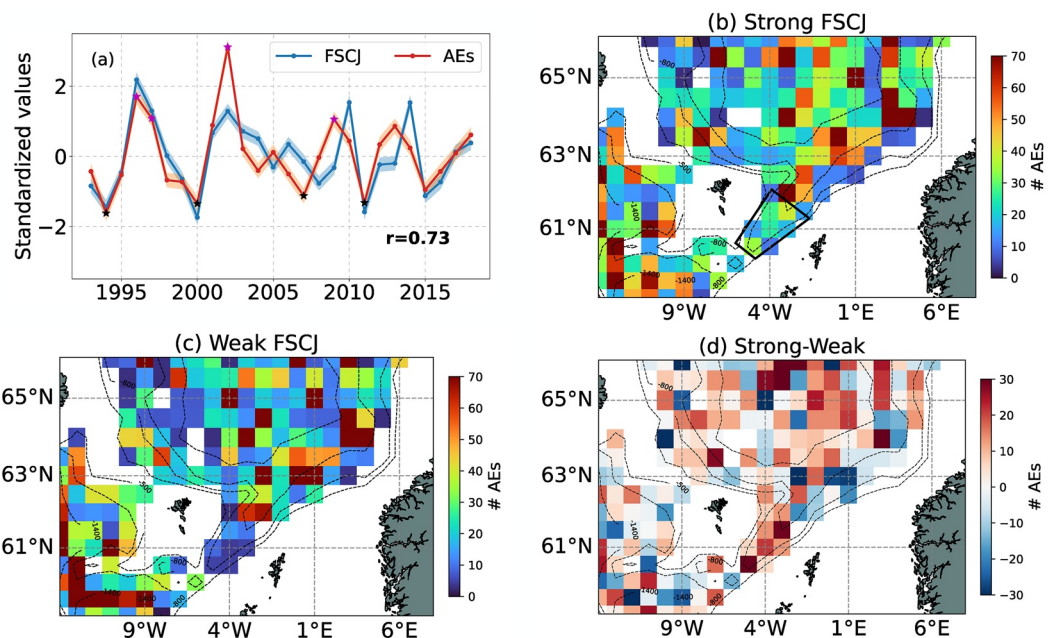


Figure 15. (a) Yearly count of anticyclonic eddies (AEs) versus Faroe-Shetland Channel Jet (FSCJ) transport between 1993 and 2018. The AEs have been detected and counted in the Faroe-Shetland Channel (FSC; see black box in panel b). The time series have been standardized. (b) Composite map of the spatial distribution of the number of AEs during years of strong FSCJ transport (higher than 1 standard deviation; purple stars in panel a). (c) Same as (b) but for years with weak FSCJ transport (<-1 standard deviation; black stars in panel a). (d) Difference between strong and weak FSCJ transport periods. The grid resolution of the density maps is $1^\circ \times 0.5^\circ$. Eddies found at depths <500 m have been masked. The dashed contours depict the 500-m, 800-m, 1,400-m, and 2,400-m isobaths.

3.7. Along-Isobath Bottom Density Gradients

On basin scales in the Nordic Seas and Arctic Ocean, the near-bottom flow is expected to be essentially aligned with the depth contours (more accurately, fH contours) and its strength and direction to be determined by the integrated wind stress along closed depth contours (Nøst & Isachsen, 2003). In the Nordic Seas and Arctic Ocean, the integrated wind-forcing tends to be cyclonic on closed depth contours, which implies that the along-isobath near-bottom flow should be cyclonic (Nøst & Isachsen, 2003). From this perspective, the deep anticyclonic FSCJ, which flows with shallow water to its right, emerges as a dynamical oddity. Thus, a relevant question is what mechanisms cause the observed deviations from the large-scale dynamical constraints in the FSC. Specifically, what dynamics are involved when the deep-water flow shifts from being cyclonic north of the Faroes to anticyclonic on the eastern side of the FSC.

The theory of Nøst and Isachsen (2003), valid for small Rossby numbers, predicts the bottom pressure $p_B = p_B(H)$ that via geostrophy gives an isobath-following bottom flow. However, if the bottom density varies along the depth contours an additional along-isobath bottom velocity arises that is also in geostrophic balance (Aaboe & Nøst, 2008; Nilsson et al., 2005). The reason is that the geostrophic velocity is related to the horizontal pressure gradient at constant z , and p_B is the pressure at $z = -H(x, y)$. This gives the following expression for the horizontal pressure gradient at $z = -H$

$$\nabla_z p(x, y, z) = \nabla p_B - \frac{\partial p}{\partial z} \nabla H \quad (2)$$

where the last term is a geometrical correction. By using the hydrostatic law ($\partial p/\partial z = -g\rho$) and the geostrophic balance Equation 2, we obtain the following expression for the along-isobath bottom velocity:

$$v = \left(-\frac{1}{f\rho_0} \frac{dp_B}{dH} + \frac{g\rho'_B}{f\rho_0} \right) |\nabla H| \quad (3)$$

where ρ'_B is the bottom buoyancy anomaly and v is counted positive for along-isobath flow with shallow water to the right (Aaboe & Nøst, 2008; Nilsson et al., 2005). Note that bottom velocity is proportional to the topographic slope $|\nabla H|$, and where the bottom density is locally higher (lower) than the isobath-mean density there will be cyclonic (anticyclonic) velocity anomalies directed along the isobaths. It is convenient to write the bottom velocity in Equation 3 as

$$v = \bar{v} + v' \quad (4)$$

where \bar{v} , proportional to $-dp_B/dH$, is determined by the integrated wind stress around closed depth contours via the model of Nøst and Isachsen (2003), and v' is the term proportional to ρ'_B . Note that generally we have $\bar{v} > 0$ (cyclonic flow) in the Nordic Seas (Aaboe & Nøst, 2008).

To examine if bottom density variations may contribute to the time-mean flow field in the FSC, we have considered the bottom density field in the ocean reanalysis (Figure 16). On the Shetland side in the FSC, the bottom density anomaly on the slope in the depth range around 800 m (a depth comparable to the FBC sill) is negative: the anomaly relative to the bottom density farther north at 63°N is -0.05 kg m^{-3} . This general feature is seen both in the World Ocean Atlas 2018 (not shown) and GLORYS12, and in the hydrographic analyses of Aaboe and Nøst (2008) and Zhou and Nøst (2013). Based on Equation 3 we expect anticyclonic bottom velocity anomalies on the order of 0.2 m s^{-1} in the FSC, where $|\nabla H| \approx 0.05$. Thus, it is possible that the locally low bottom density anomaly can partly explain the southward flow on the Shetland side in the FSC, i.e., $v' + \bar{v} < 0$. This explanation of the anticyclonic near-bottom flow in the FSC fits also qualitatively with the idea that the integrated wind stress on closed depth contours in the Nordic Seas modulate the deep flow: stronger (weaker) \bar{v} coincides with periods of stronger (weaker) cyclonic wind forcing. These results are qualitatively consistent with bottom density distributions in GLORYS12.

We emphasize that if the Rossby number characterizing the flow locally grows toward or beyond unity, it will become less constrained by the topography. Larger Rossby numbers of flow along a slope are expected where the slope or the curvature of the topography becomes large (Broomé & Nilsson, 2016; Nøst et al., 2008). Near such topographic features, the along-slope flow may become unstable, shed eddies, and partly detach from the

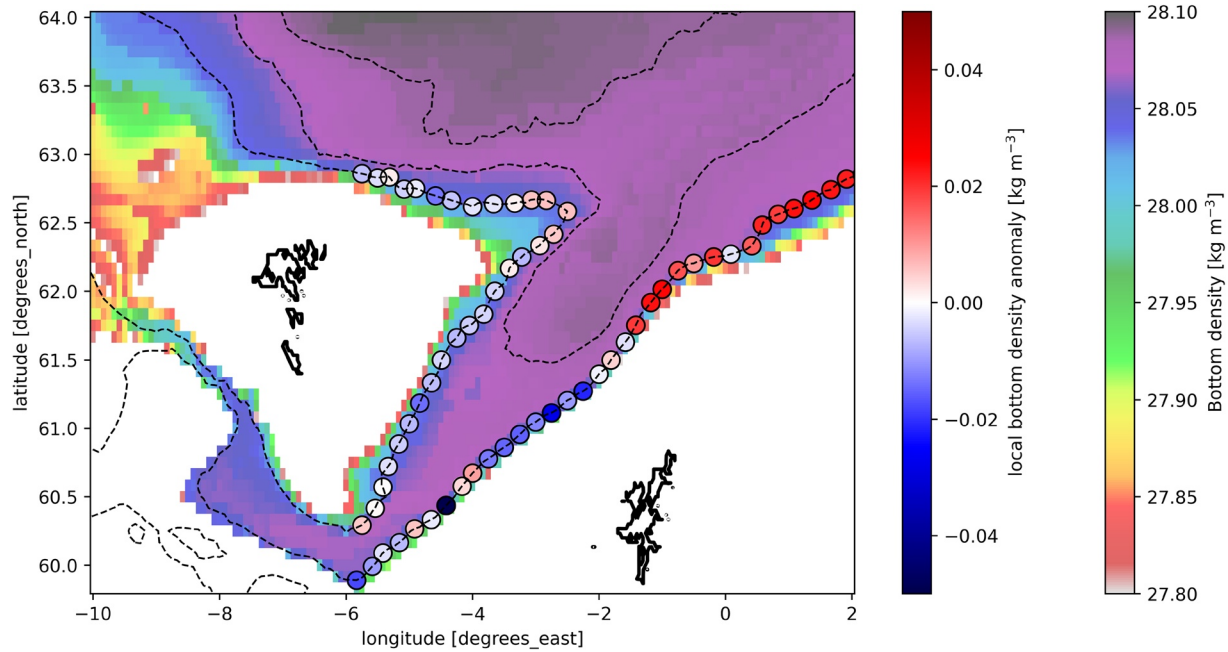


Figure 16. Bottom density from the GLORYS12 ocean reanalysis (colors). The circles show the bottom density anomaly (red-blue color scale), calculated as the local bottom density minus the along-isobath mean bottom density in the Faroe-Shetland Channel (along the 800-m isobath at the circles). The dashed contours depict the 800-m, 1,400-m, and 2,400-m isobaths.

slope. Such nonlinear effects are likely to be important for the flow in the FSC, where steep slopes and high curvature are found in the topography (e.g., Sjøiland et al., 2008). Despite complex dynamics on the regional scale, the time-mean near-bottom flow in the FSC may still be modulated by the large-scale wind forcing over the Nordic Seas approximately as expected from the linear theory of Nøst and Isachsen (2003) (see also Figure 14).

4. Summary and Conclusions

We have, in the present study, focused on the structure, variability, and driving mechanisms of the FSCJ, i.e., the main conduit of overflow water feeding the lower branch of the AMOC via the FBC, using a high-resolution ocean reanalysis (GLORYS12). This product has proven to be promising regarding several aspects of the circulation in the region and can thus be used to study the dense water pathways approaching the FSC and improve our understanding of the associated dynamics and spatiotemporal variability.

We have shown that both GLORYS12 and an ensemble of coarse-resolution ocean reanalyses agree well regarding the observed location of the FSCJ, i.e., banked against the Shetland slope under the main core of the Atlantic inflow. Regarding the evaluation of the hydrographic structure, GLORYS12 compares well with the time-mean hydrography from a standard section in the FSC. GLORYS12 was also shown to capture in considerable detail the velocity structure in the top 600 m when compared with directly measured ADCP velocities from a ship in regular service. While we could only find three Argo floats that passed through the FSC, we note that these generally tended to trace the GLORYS12 FSCJ path before escaping through the FBC. A similar behavior in the pathways was observed from the cluster of floats released north of the Iceland-Faroe-Ridge that later exited the FBC (Sjøiland et al., 2008).

On seasonal and longer time scales, FSCJ transport variations appear to be substantially governed or shaped by wind forcing over the Nordic Seas. A similar result was found for the FBCO as reported by Bringedal et al. (2018). Furthermore, on seasonal time scales, we found that the phasing of the FSCJ transport aligns somewhat better than the deep FSC transport against the observed FBCO transport. This suggests that on seasonal time scales, there is good temporal coherency between the FSCJ and the FBCO transport variability.

On interannual time scales, we found a strong relationship between the FSCJ transport and the entire velocity field across the FSC. This pattern appears to be controlled by the large-scale wind forcing in the North Atlantic and Nordic Seas via the changes in the storm tracks. During a southerly shift of the storm tracks, the atmospheric/ocean circulation in the Nordic Seas weakens, which leads to a decrease in the Shetland Slope Current and an increase in the FSCJ transport. Furthermore, and because of the largely barotropic structure across the FSC, variations in the FSCJ transport can be detected from satellite sea-surface heights locally in the interior FSC. This close correspondence thus provides us with an indirect measure from satellite altimetry of the deep flows in the FSC.

The temporal variability of the number of AEs generated in the FSC region was found to be strongly correlated with the FSCJ transport. The enhanced generation of anticyclonic during these years could play an active role in supplying water to the overflow-feeding jet, thereby modulating the overflow transport toward the FBC. However, the detailed mechanisms by which AEs influence the FSCJ are still not clear and will require further study.

Finally, the theoretical consideration presented in Section 3.7 suggests that the FSCJ is qualitatively consistent with geostrophic balance given the decreasing bottom density anomaly field in the downstream direction of the FSCJ. The dynamics that set the density field and the anticyclonic FSCJ flow likely involve ageostrophic effects and eddy-mean flow interactions, and would be interesting to examine in future studies.

Data Availability Statement

The DUACS DT2018 SSH data described in Taburet et al. (2019) are from the Copernicus Marine Environment Monitoring Service (CMEMS) and can be accessed through this link: <https://resources.marine.copernicus.eu/products>. The ERA-Interim data described in Dee et al. (2011) can be found here: <https://www.ecmwf.int/en/forecasts/datasets/reanalysis-datasets/era-interim>. The CMEMS GLORYS12 ocean reanalysis, <https://doi.org/10.48670/moi-00021>, described in Jean-Michel et al. (2021) can be accessed here: https://resources.marine.copernicus.eu/product-detail/GLOBAL_MULTIYEAR_PHY_001_030/INFORMATION. The CMEMS global ocean ensemble reanalyses, <https://doi.org/10.48670/moi-00023>, can be accessed from here: https://resources.marine.copernicus.eu/product-detail/GLOBAL_REANALYSIS_PHY_001_026/INFORMATION. The Nolso-Flugga hydrography by Larsen et al. (2018), <https://doi.org/10.7489/12056-1>, can be downloaded through this link: <https://data.marine.gov.scot/dataset/temperature-and-salinity-ctd-data-nolso-flugga-section>. The ARGO floats identified using the argopy software by Maze and Balem (2020), can be downloaded from here: https://www.nodc.noaa.gov/argo/floats_data.htm. The Norröna data described in Rossby and Flagg (2012) and Rossby et al. (2018) are available through this link: <http://po.msrc.sunysb.edu/Norröna/>. The AVISO atlas by Pegliasco et al. (2022) can be accessed through this link: <https://www.aviso.altimetry.fr/en/data/products/value-added-products/global-mesoscale-eddy-trajectory-product/meta3-2-dt.html>. The Faroe-Bank Channel overflow data described in Hansen et al. (2016) were made available by the Faroe Marine Research Institute: <http://www.envofar.fo/index.php?page=climate>.

References

- Aaboe, S., & Nøst, O. A. (2008). A diagnostic model of the Nordic Seas and Arctic Ocean circulation: Quantifying the effects of a variable bottom density along a sloping topography. *Journal of Physical Oceanography*, 38(12), 2685–2703. <https://doi.org/10.1175/2008jpo3862.1>
- Berx, B., Hansen, B., Østerhus, S., Larsen, K. M., Sherwin, T., & Jochumsen, K. (2013). Combining in-situ measurements and altimetry to estimate volume, heat and salt transport variability through the Faroe Shetland Channel. *Ocean Science Discussions*, 10(1), 153–195. <https://doi.org/10.5194/os-9-639-2013>
- Bringedal, C., Eldevik, T., Skagseth, Ø., Spall, M. A., & Østerhus, S. (2018). Structure and forcing of observed exchanges across the Greenland-Scotland Ridge. *Journal of Climate*, 31(24), 9881–9901. <https://doi.org/10.1175/jcli-d-17-0889.1>
- Broomé, S., & Nilsson, J. (2016). Stationary sea surface height anomalies in cyclonic boundary currents: Conservation of potential vorticity and deviations from strict topographic steering. *Journal of Physical Oceanography*, 46(8), 2437–2456. <https://doi.org/10.1175/jpo-d-15-0219.1>
- Chafik, L. (2012). The response of the circulation in the Faroe-Shetland Channel to the North Atlantic Oscillation. *Tellus*, 64, 18423. <https://doi.org/10.3402/tellusa.v64i0.18423>
- Chafik, L., Hátún, H., Kjellsson, J., Larsen, K. M. H., Rossby, T., & Berx, B. (2020). Discovery of an unrecognized pathway carrying overflow waters toward the Faroe Bank Channel. *Nature Communications*, 11(1), 3721. <https://doi.org/10.1038/s41467-020-17426-8>
- Chafik, L., & Rossby, T. (2019). Volume, heat, and freshwater divergences in the subpolar North Atlantic suggest the Nordic Seas as key to the state of the meridional overturning circulation. *Geophysical Research Letters*, 46, 4799–4808. <https://doi.org/10.1029/2019GL082110>
- Chelton, D. B., DeSzoeke, R. A., Schlax, M. G., El Naggar, K., & Siwertz, N. (1998). Geographical variability of the first baroclinic Rossby radius of deformation. *Journal of Physical Oceanography*, 28(3), 433–460. [https://doi.org/10.1175/1520-0485\(1998\)028<0433:gvoftb>2.0.co;2](https://doi.org/10.1175/1520-0485(1998)028<0433:gvoftb>2.0.co;2)
- Dee, D. P., Uppala, S. M., Simmons, A. J., Berrisford, P., Poli, P., Kobayashi, S., et al. (2011). The ERA-Interim reanalysis: Configuration and performance of the data assimilation system. *Quarterly Journal of the Royal Meteorological Society*, 137(656), 553–597. <https://doi.org/10.1002/qj.828>

Acknowledgments

This work was supported by grants from the Swedish National Space Agency (Dnr 133/17, 2020-00171, 2022-00172). The authors wish to thank the two reviewers for their careful review and constructive comments that greatly improved our study.

- Eldevik, T., Nilsen, J. E. Ø., Iovino, D., Anders Olsson, K., Sandø, A. B., & Drange, H. (2009). Observed sources and variability of Nordic Seas overflow. *Nature Geoscience*, 2(6), 406–410. <https://doi.org/10.1038/ngeo518>
- Hansen, B., Larsen, K. M. H., Hátún, H., & Østerhus, S. (2016). A stable Faroe Bank Channel overflow 1995–2015. *Ocean Science*, 12(6), 1205–1220. <https://doi.org/10.5194/os-12-1205-2016>
- Hansen, B., & Østerhus, S. (2000). North Atlantic-Nordic Seas exchanges. *Progress in Oceanography*, 45(2), 109–208. [https://doi.org/10.1016/S0079-6611\(99\)00052-X](https://doi.org/10.1016/S0079-6611(99)00052-X)
- Hátún, H., Chafik, L., & Larsen, K. M. H. (2021). The Norwegian Sea gyre—A regulator of Iceland-Scotland Ridge exchanges. *Frontiers in Marine Science*, 8, 694614. <https://doi.org/10.3389/fmars.2021.694614>
- Huang, J., Pickart, R. S., Huang, R. X., Lin, P., Brakstad, A., & Xu, F. (2020). Sources and upstream pathways of the densest overflow water in the Nordic Seas. *Nature Communications*, 11(1), 5389. <https://doi.org/10.1038/s41467-020-19050-y>
- Jean-Michel, L., Eric, G., Romain, B.-B., Gilles, G., Angélique, M., Marie, D., et al. (2021). The Copernicus global 1/12 oceanic and sea ice GLORYS12 reanalysis. *Frontiers of Earth Science*, 9, 698876. <https://doi.org/10.3389/feart.2021.698876>
- Jonsson, S., & Valdimarsson, H. (2004). A new path for the Denmark Strait overflow water from the Iceland Sea to Denmark Strait. *Geophysical Research Letters*, 31, L03305. <https://doi.org/10.1029/2003GL019214>
- Larsen, K., Berx, B., Hátún, H., Hindson, J., & Jochumsen, K. (2018). Havstovan Group and Marine Scotland Science Oceanography Group. Temperature and salinity on the Nolso-Flugga (NWE) standard hydrographic section, part of the Faroe-Shetland Channel transport mooring array [Dataset]. <https://doi.org/10.7489/12056-1>
- Lozier, M. S. (2012). Overturning in the North Atlantic. *Annual Review of Marine Science*, 4(1), 291–315. <https://doi.org/10.1146/annurev-marine-120710-100740>
- Mason, E., Pascual, A., & McWilliams, J. C. (2014). A new sea surface height-based code for oceanic mesoscale eddy tracking. *Journal of Atmospheric and Oceanic Technology*, 31(5), 1181–1188. <https://doi.org/10.1175/jtech-d-14-00019.1>
- Mauritzen, C. (1996). Production of dense overflow waters feeding the North Atlantic across the Greenland-Scotland Ridge. Part 1: Evidence for a revised circulation scheme. *Deep Sea Research Part I: Oceanographic Research Papers*, 43(6), 769–806. [https://doi.org/10.1016/0967-0637\(96\)00037-4](https://doi.org/10.1016/0967-0637(96)00037-4)
- Maze, G., & Balem, K. (2020). argopy: A Python library for Argo ocean data analysis. *Journal of Open Source Software*, 5(33), 2425. <https://doi.org/10.21105/joss.02425>
- McKenna, C., Berx, B., & Austin, W. (2016). The decomposition of the Faroe-Shetland Channel water masses using parametric optimum multi-parameter analysis. *Deep Sea Research Part I: Oceanographic Research Papers*, 107, 9–21. <https://doi.org/10.1016/j.dsr.2015.10.013>
- Nilsson, J., Walin, G., & Broström, G. (2005). Thermohaline circulation induced by bottom friction in sloping-boundary basins. *Journal of Marine Research*, 63(4), 705–728. <https://doi.org/10.1357/0022240054663222>
- Nøst, O. A., & Isachsen, P. E. (2003). The large-scale time-mean ocean circulation in the Nordic Seas and Arctic Ocean estimated from simplified dynamics. *Journal of Marine Research*, 61(2), 175–210. <https://doi.org/10.1357/002224003322005069>
- Nøst, O. A., Nilsson, J., & Nycander, J. (2008). On the asymmetry between cyclonic and anticyclonic flow in basins with sloping boundaries. *Journal of Physical Oceanography*, 38(4), 771–787. <https://doi.org/10.1175/2007jpo3714.1>
- Oey, L.-Y. (1997). Eddy energetics in the Faroe-Shetland Channel: A model resolution study. *Continental Shelf Research*, 17(15), 1929–1944. [https://doi.org/10.1016/S0278-4343\(97\)00053-8](https://doi.org/10.1016/S0278-4343(97)00053-8)
- Østerhus, S., Woodgate, R., Valdimarsson, H., Turrell, B., de Steur, L., Quadfasel, D., et al. (2019). Arctic Mediterranean exchanges: A consistent volume budget and trends in transports from two decades of observations. *Ocean Science*, 15(2), 379–399. <https://doi.org/10.5194/os-15-379-2019>
- Pegliasco, C., Delepouille, A., Mason, E., Morrow, R., Faugère, Y., & Dibarboire, G. (2022). META3.1exp: A new global mesoscale eddy trajectory atlas derived from altimetry. *Earth System Science Data*, 14(3), 1087–1107. <https://doi.org/10.5194/essd-14-1087-2022>
- Rosby, T., Chafik, L., & Houpert, L. (2020). What can hydrography tell us about the strength of the Nordic Seas MOC over the last 70 to 100 years? *Geophysical Research Letters*, 47, e2020GL087456. <https://doi.org/10.1029/2020GL087456>
- Rosby, T., Flagg, C., Chafik, L., Harden, B., & Sjøiland, H. (2018). A direct estimate of volume, heat, and freshwater exchange across the Greenland-Iceland-Faroe-Scotland Ridge. *Journal of Geophysical Research: Oceans*, 123, 7139–7153. <https://doi.org/10.1029/2018JC014250>
- Rosby, T., & Flagg, C. N. (2012). Direct measurement of volume flux in the Faroe-Shetland Channel and over the Iceland-Faroe ridge. *Geophysical Research Letters*, 39, L07602. <https://doi.org/10.1029/2012GL051269>
- Semper, S., Pickart, R. S., Våge, K., Larsen, K. M. H., Hátún, H., & Hansen, B. (2020). The Iceland-Faroe Slope Jet: A conduit for dense water toward the Faroe Bank Channel overflow. *Nature Communications*, 11(1), 5390. <https://doi.org/10.1038/s41467-020-19049-5>
- Sherwin, T. J., Turrell, W. R., Jeans, D. R. G., & Dye, S. (1999). Eddies and a mesoscale deflection of the slope current in the Faroe-Shetland Channel. *Deep Sea Research Part I: Oceanographic Research Papers*, 46(3), 415–438. [https://doi.org/10.1016/S0967-0637\(98\)00077-6](https://doi.org/10.1016/S0967-0637(98)00077-6)
- Sherwin, T. J., Williams, M. O., Turrell, W. R., Hughes, S. L., & Miller, P. I. (2006). A description and analysis of mesoscale variability in the Fåroe-Shetland Channel. *Journal of Geophysical Research*, 111, C03003. <https://doi.org/10.1029/2005JC002867>
- Sjøiland, H., Prater, M., & Rosby, T. (2008). Rigid topographic control of currents in the Nordic Seas. *Geophysical Research Letters*, 35, L18607. <https://doi.org/10.1029/2008GL034846>
- Taburet, G., Sanchez-Roman, A., Ballarotta, M., Pujol, M.-I., Legeais, J.-F., Fournier, F., et al. (2019). Duacs DT2018: 25 years of reprocessed sea level altimetry products. *Ocean Science*, 15(5), 1207–1224. <https://doi.org/10.5194/os-15-1207-2019>
- Timmermans, M.-L., & Marshall, J. (2020). Understanding Arctic Ocean circulation: A review of ocean dynamics in a changing climate. *Journal of Geophysical Research: Oceans*, 125, e2018JC014378. <https://doi.org/10.1029/2018JC014378>
- Våge, K., Pickart, R. S., Spall, M. A., Valdimarsson, H., Jónsson, S., Torres, D. J., et al. (2011). Significant role of the North Icelandic Jet in the formation of Denmark Strait overflow water. *Nature Geoscience*, 4(10), 723–727. <https://doi.org/10.1038/ngeo1234>
- Woollings, T., Gregory, J. M., Pinto, J. G., Reyers, M., & Brayshaw, D. J. (2012). Response of the North Atlantic storm track to climate change shaped by ocean-atmosphere coupling. *Nature Geoscience*, 5(5), 313–317. <https://doi.org/10.1038/ngeo1438>
- Yang, J., & Pratt, L. J. (2013). On the effective capacity of the dense-water reservoir for the Nordic Seas overflow: Some effects of topography and wind stress. *Journal of Physical Oceanography*, 43(2), 418–431. <https://doi.org/10.1175/jpo-d-12-087.1>
- Yang, J., & Pratt, L. J. (2014). Some dynamical constraints on upstream pathways of the Denmark Strait overflow. *Journal of Physical Oceanography*, 44(12), 3033–3053. <https://doi.org/10.1175/jpo-d-13-0227.1>
- Zhang, R., Delworth, T. L., Rosati, A., Anderson, W. G., Dixon, K. W., Lee, H.-C., & Zeng, F. (2011). Sensitivity of the North Atlantic Ocean Circulation to an abrupt change in the Nordic Sea overflow in a high resolution global coupled climate model. *Journal of Geophysical Research*, 116, C12024. <https://doi.org/10.1029/2011JC007240>
- Zhou, Q., & Nøst, O. A. (2013). The establishment of Atlantic Water transport as a topographically trapped slope current off Scotland. *Tellus A: Dynamic Meteorology and Oceanography*, 65(1), 19978. <https://doi.org/10.3402/tellusa.v65i0.19978>